

Chord length sampling with memory effects for spatially heterogeneous Markov media: Application to the rod model

A. Tentori^{1,*}, C. Larmier¹, J. Durand², B. Cochet² and A. Zoia¹

¹Université Paris-Saclay, CEA, Service d'études des réacteurs et de mathématiques appliquées, 91191 Gif-sur-Yvette, France

²CEA, DAM, DIF, Arpajon, F-91297, France



(Received 24 October 2023; accepted 7 February 2024; published 19 March 2024)

In this work we propose a modified Chord Length Sampling (CLS) algorithm, endowed with two layers of “memory effects,” aimed at solving particle transport problems in one-dimensional spatially nonhomogeneous Markov media. CLS algorithms are a family of Monte Carlo methods which account for the stochastic nature of the media by sampling on-the-fly the random interfaces between material phases during the particle propagation. The possibility for the particles to remember the last crossed interfaces increases the accuracy of these models with respect to reference solutions obtained by solving the Boltzmann equation on a large number of realizations of the Markov media. In previous investigations, CLS models with memory have been tested exclusively for spatially uniform stochastic media: in this paper we extend this class of Monte Carlo methods to the case of spatially nonhomogeneous configurations. The effectiveness and the robustness of the modified CLS are probed considering several benchmark problems with varying material cross sections and Markov media densities. The obtained results are a stepping stone towards a generalization to three-dimensional models.

DOI: [10.1103/PhysRevE.109.035302](https://doi.org/10.1103/PhysRevE.109.035302)

I. INTRODUCTION

In the last three decades, considerable efforts have been devoted to modeling particle transport in stochastic mixtures [1]. A stochastic mixture is a medium consisting of two or more immiscible components,¹ arranged randomly in space according to given statistical laws [2]. The material properties of the medium in which particles propagate are known only statistically, and one is required to assign the probability $p_\alpha(\mathbf{r})$ of finding material α at position \mathbf{r} .

Such complex systems occur in several applications of nuclear engineering, including inertial confinement fusion (ICF), fission reactor physics, and radiation shielding problems. In particular, the pioneering works on random media aimed at providing a theoretical framework and numerical tools to investigate the transport of photons through the Rayleigh-Taylor instabilities, in the context of ICF [1,3–8]. Stochastic media have received attention in the modeling of neutron transport within high-temperature gas-cooled reactors (HTGRs), where microspheres of fissile material are randomly dispersed into graphite pellets [9–12]. In the domain of neutron transport, random media are also relevant in the modeling of fluid-vapor mixtures in boiling water reactors (BWRs) [13], in radiation shielding problems involving composite materials [14–16], and in criticality safety issues, e.g., after severe accidents [17,18].

Several models of random media have been proposed, each with distinct features. In the field of particle transport applications, a useful classification of stochastic mixtures is

based on the distribution $f_\alpha(s|\mathbf{r}, \boldsymbol{\Omega})$ of chord lengths s of each model, generated by intersecting an arbitrary line in direction $\boldsymbol{\Omega}$ at position \mathbf{r} placed into the medium with the interfaces of the random regions of material α that compose the mixture. Since particle transport is based on a series of flights having exponentially distributed lengths between collision events, the comparison between the distribution of the flight lengths and the one of the chord lengths is an appropriate metric of the impact of random media on the particle histories [1].

In this respect, a peculiar class of mixing statistics widely used for particle transport problems is that of *Markov media* [1,19], which are characterized by exponentially distributed chord lengths

$$f_\alpha(s|\mathbf{r}, \boldsymbol{\Omega}) = \rho_\alpha(\mathbf{r} + s\boldsymbol{\Omega}, \boldsymbol{\Omega})e^{-\int_0^s ds' \rho_\alpha(\mathbf{r} + s'\boldsymbol{\Omega}, \boldsymbol{\Omega})}, \quad (1)$$

whose single free parameter is the total transition rate $\rho_\alpha(\mathbf{r}, \boldsymbol{\Omega})$, which corresponds to the probability per unit length of crossing the interface of material α . Note that $\rho_\alpha(\mathbf{r}, \boldsymbol{\Omega})$ generally depends on both the direction $\boldsymbol{\Omega}$ and the position \mathbf{r} , which corresponds to spatially heterogeneous and non-isotropic Markov media. In the simpler case of spatially homogeneous mixing statistics, transition rates take the form $\rho_\alpha(\mathbf{r}, \boldsymbol{\Omega}) = \rho_\alpha(\boldsymbol{\Omega})$, and if we further assume that the media are isotropic $\rho_\alpha(\boldsymbol{\Omega}) = \rho_\alpha$ are constant.

An exact approach to model particle transport in random media consists in sampling a sufficiently large ensemble of medium realizations from the mixing statistics and then solving the Boltzmann transport equation for each realization. The ensemble average over all the obtained solutions provides an unbiased estimate of the sought physical observables; however, this comes at the expense of a very high computational effort. Therefore, the possibility of deriving homogenized models enabling faster, albeit approximate results is of utmost importance for industrial applications. In order for such

*alessandro.tentori@cea.fr; alessandro.tentori@mail.polimi.it

¹Generally speaking, the mixture can be made of composite materials, or the same material in different physical states.

“effective” models to be robust and reliable, the bias with respect to the exact approach must be carefully assessed: this can be achieved by developing a solid theoretical framework, and by performing extensive validation against reference solutions.

For Markov media, a well-known effective transport model is based on the Levermore-Pomraning (LP) equations [4,20], which stem from taking the ensemble average of the Boltzmann equation over the random material realizations and truncating the resulting infinite hierarchy of equations by assuming that the mean flux at the interface between two material chunks in the mixture is equal to the mean flux within the chunk. This assumption is formally exact for purely absorbing media, but fails when scattering is present. The LP equations can be solved either by deterministic [21,22] or Monte Carlo methods. The Monte Carlo algorithm which solves the LP system is the so-called Chord Length Sampling (CLS) method, proposed by Zimmerman and Adams [23,24]. CLS closely resembles the regular flight-collision Markov process associated to the Boltzmann equation, but particles are further assigned a material index α that is switched on the fly by sampling fictitious random material interfaces along the flights.

The memoryless nature of the material interfaces in the standard CLS hinders the preservation of spatial correlations, and accounts for the occurrence of a systematical bias with respect to reference solutions. The strength of the bias depends on the ratio $\rho_\alpha/\Sigma_{t,\alpha}$, where $\Sigma_{t,\alpha}$ is the total cross section for material α . Pioneering works in one-dimensional implementations have shown that the introduction of “memory effects,” with particles keeping partial track of the interfaces already crossed along their history, can improve the accuracy of CLS [22,23].

Over the last decade, significant progress has been made in the analysis of Markov media. Algorithms enabling the Monte Carlo sampling of spatially homogeneous three-dimensional realizations have been proposed, based on a generalization of the Switzer procedure, and their statistical properties have been thoroughly investigated [25–27]. Due to these advances, the key features of particle transport through three-dimensional Markov media have been explored, and reference (ensemble-averaged) solutions have been obtained for a variety of configurations, encompassing a revisited version of the celebrated Adams, Larsen, and Pomraning benchmark [28,29]. Such solutions have been then used to assess the accuracy of the CLS method [30]. Furthermore, in order to overcome the limitations of the CLS approach, three-dimensional CLS-like models including memory effects were developed, such as Poisson-Box Sampling [31] and the Local Realization Preserving [32], which rely on some form of bookkeeping of the previously crossed material surfaces. Both strategies have been shown to considerably decrease the discrepancy with respect to reference solutions.

Recently, attention has shifted towards the case of Markov media with spatial gradients, which are key to real-world applications. The one-dimensional case has been considered in Refs. [33,34], and the three-dimensional case (including a comparison with spatially heterogeneous CLS) has been examined in Refs. [35,36]. In particular, these latter findings showed the limited capability of CLS algorithm to accurately approximate reference solutions in heterogeneous

configurations. Therefore, in view of the results obtained in the spatially homogeneous case, it would be highly desirable to add memory effects to CLS in the broader class of Markov media with spatial gradients.

The goal of this paper is to propose a strategy to endow CLS with memory effects in a general spatially heterogeneous setting. In order to keep the implementation framework simple, and yet preserve all the relevant features of this class of models, we choose to work with one-dimensional systems. For this purpose, a CLS-like algorithm including two layers of memory effects will be developed and its accuracy will be tested against reference solutions obtained for Markov media with arbitrary spatial gradients. The choice of one-dimensional configurations is motivated by three considerations. First, CLS-like algorithms with memory such as the Poisson-Box Sampling or Local Realization Preserving method heavily rely on the relative orientation of the material surfaces kept in memory by the particles, which would lead to a nontrivial interplay with the angular dependence of the transition rates $\rho_\alpha(\mathbf{r}, \boldsymbol{\Omega})$ in spatially heterogeneous configurations. In this respect, the one-dimensional rod model, where particle directions can take only two values, allows probing the proposed implementation for stochastic media with spatial gradients without being hindered by the full complexity of the angular dependence. Second, one-dimensional Markov media allow finely tuning spatial gradients in both the color probability and the spatial scale, contrary to higher-dimensional media where explicit constructions based on stochastic tessellations are inherently limited to gradients in the spatial scale [36]. Finally, it is widely acknowledged that standard CLS algorithms are less accurate in one-dimensional problems: due to the increased probability of back-scattering, particles can more often revisit material regions whose interfaces have been forgotten because of the memoryless nature of the sampling. Therefore, it is interesting to assess the positive impact brought by the introduction of memory effects in these configurations.

This paper is structured as follows: in Sec. II we first recall the mathematical properties of one-dimensional Markov media and the main algorithms for the sampling of random configurations. The statistical features of the sampled Markov media will be probed by comparison with theoretical predictions. Particle transport in Markov media will be presented in Sec. III, where we will discuss both reference solutions based on ensemble averages and the CLS approach. For this latter, we will detail a strategy enabling two layers of memory effects with general space and direction-dependent transition rates $\rho_\alpha(\mathbf{r}, \boldsymbol{\Omega})$. Then in Sec. IV we will compare the results of CLS with and without memory effects against reference solutions: simulation results will be reported for a few relevant benchmark configurations. Conclusions will be finally drawn in Sec. V.

II. ONE-DIMENSIONAL MARKOV MIXTURES

We begin by reviewing the main statistical properties of one-dimensional Markov mixtures and the Monte Carlo methods used to sample the corresponding realizations. For the purpose of probing the reliability of our implementation, which is key for the generation of the reference solutions needed for the verification of the CLS methods, we will compare the probabilities p_α and the transition rates ρ_α estimated

from the sampled realizations to the exact results stemming from the theory of Markov media. Special emphasis will be given to the case of spatially heterogeneous media.

A. Statistical properties

The statistical properties of one-dimensional Markov media have been extensively examined [1,4,21,37]. For a recent survey, see, e.g., [36]. In the following, we limit ourselves to recalling the main theoretical results that are useful for our purposes.

Markov media are defined in terms of a Markov jump process over a collection of discrete states $\alpha = \{0, 1, \dots\}$, with transition rates $\rho_{\alpha,\beta}(x, \Omega_{\pm})$ representing the probabilities per unit length to have a transition from material α to material $\beta \neq \alpha$, at position x in the direction Ω_{\pm} , and the initial condition $p_{\alpha}(x_0)$. Clearly, in dimension $d = 1$, the only allowed directions are either $\Omega_- = -1$ or $\Omega_+ = +1$. The total transition rate reads

$$\rho_{\alpha}(x, \Omega_{\pm}) = \sum_{\beta \neq \alpha} \rho_{\alpha,\beta}(x, \Omega_{\pm}), \quad (2)$$

and the one-dimensional chord length distribution can be consequently written as

$$f_{\alpha}(s|x, \Omega_{\pm}) = \rho_{\alpha}(x + s\Omega_{\pm}, \Omega_{\pm}) e^{-\int_0^s ds' \rho_{\alpha}(x+s'\Omega_{\pm}, \Omega_{\pm})}. \quad (3)$$

Another relevant quantity is the color probability $p_{\alpha}(x)$, defined as the probability to find material α at position x (the word ‘‘color’’ is used as synonym for material), which obeys a set of coupled Chapman-Kolmogorov equations:

$$\pm \frac{\partial}{\partial x} p_{\alpha}(x) = \sum_{\beta \neq \alpha} p_{\beta}(x) \rho_{\beta,\alpha}(x, \Omega_{\pm}) - p_{\alpha}(x) \rho_{\alpha}(x, \Omega_{\pm}). \quad (4)$$

Forward and backward rates are related to the color probabilities by an elegant symmetry condition [37], namely,

$$p_{\alpha}(x) \rho_{\alpha,\beta}(x, \Omega_{\pm}) = p_{\beta}(x) \rho_{\beta,\alpha}(x, \Omega_{\mp}). \quad (5)$$

For the special case of binary mixtures, Eq. (4) for direction Ω_+ has the simple solution

$$p_{\alpha}(x) = p_{\alpha}(x_0) e^{-\int_{x_0}^x \hat{\rho}(u, \Omega_+) du} + \int_{x_0}^x \rho_{\beta}(z, \Omega_+) e^{-\int_z^x \hat{\rho}(u, \Omega_+) du} dz, \quad (6)$$

where

$$\hat{\rho}(x, \Omega_{\pm}) = \rho_{\alpha}(x, \Omega_{\pm}) + \rho_{\beta}(x, \Omega_{\pm}), \quad (7)$$

with $\alpha = \{0, 1\}$ and $p_{\alpha}(x) = 1 - p_{\beta}(x)$, $\beta \neq \alpha$.

B. Sampling and verification of Markov media

In order to sample one-dimensional Markov media by Monte Carlo methods, we use the ‘‘sweeping’’ technique recalled in [36]. Let us assume that the line has a finite length L , say, in the interval $[-L/2, L/2]$. The sweeping in direction Ω_+ begins from the left boundary of the rod, $x_0 = -L/2$: the color of the first material chunk is sampled from the initial condition $p_{\alpha}(-L/2)$. For sake of simplicity, for all the configurations considered in this work, initial conditions are chosen in order to preserve equilibrium at the left boundary, i.e.,

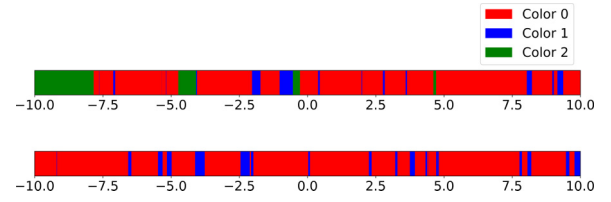


FIG. 1. Two realizations of one-dimensional Markov mixtures on the segment $[-L/2, L/2]$, sampled using the sweeping algorithm described in Sec. II B. Top: Homogeneous Markov mixing of three materials, with transition rates $\rho_{0,1} = 100/99$, $\rho_{0,2} = 10/99$, $\rho_{1,0} = 100/11$, $\rho_{1,2} = 10/11$, $\rho_{2,0} = 100/55$, and $\rho_{2,1} = 10/55$, and initial conditions $p_0 = 0.833$, $p_1 = 0.085$, and $p_2 = 0.081$, respectively. Bottom: Homogeneous Markov mixing of two materials, with transition rates $\rho_{0,1} = 100/99$ and $\rho_{1,0} = 100/11$, and initial condition $p_0(-L/2) = 0.9$. In both cases the rod length is $L = 20$.

ensuring that p_{α} remains constant in the right neighborhood of $-L/2$: $p_{\alpha}(-L/2) = p_{\alpha}(-L/2 + dx)$, with $dx \rightarrow 0$. This is achieved by choosing p_{α} so that

$$\sum_{\beta \neq \alpha} p_{\beta}(x) \rho_{\beta,\alpha}(x, \Omega_+) = p_{\alpha}(x) \rho_{\alpha}(x, \Omega_+) \quad (8)$$

for $x = -L/2$, which follows from Eq. (4). The length of the first chunk is then sampled from the nonhomogeneous exponential probability density in Eq. (3), with parameter $\rho_{\alpha}(x, \Omega_+)$, e.g., using the ‘‘thinning’’ method [38]. The position of the interface x_{α} of color α is saved, and the color $\beta \neq \alpha$ of the next chunk is sampled from the transition probability

$$P_{\alpha \rightarrow \beta}(x_{\alpha}, \Omega_+) = \frac{\rho_{\alpha,\beta}(x_{\alpha}, \Omega_+)}{\rho_{\alpha}(x_{\alpha}, \Omega_+)}. \quad (9)$$

The process is repeated and segments are added until the right boundary of the interval is reached. In the case of binary mixtures, $\rho_{\alpha,\beta} = \rho_{\alpha}$ and $P_{\alpha \rightarrow \beta} = 1$, with $\beta \neq \alpha$. For illustration, Fig. 1 shows two realizations of one-dimensional homogeneous Markov media. The sweeping procedure can be equivalently applied in the reversed direction, in which case the initial condition would be assigned at the right boundary of the segment.

For the purpose of testing the correct implementation of the sweeping algorithm, we have compared the statistical features of the sampled realizations to the theoretical predictions reported in the previous section. A large collection of realizations is sampled and the ensemble averages of some relevant observables are estimated at different positions x_k of the rod. Generally, the ensemble average of an observable O over M realizations is estimated as

$$\bar{O} = \frac{1}{M} \sum_{m=1}^M O_m, \quad (10)$$

where O_m is the value sampled on the m th realization. The associated statistical uncertainty is

$$\sigma_G^2(\bar{O}) = \frac{1}{M-1} \left[\frac{1}{M} \sum_{m=1}^M O_m^2 - \bar{O}^2 \right]. \quad (11)$$

We have considered as observables the color probability and the transition rates. For the former, we use as a natural

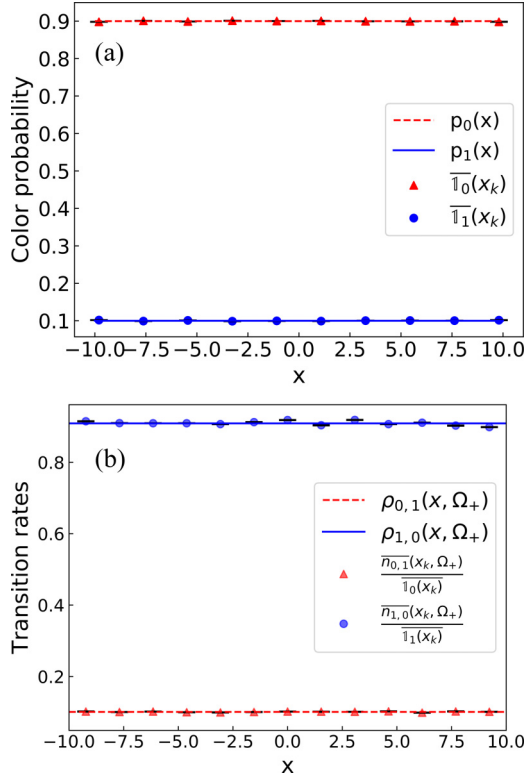


FIG. 2. (a) Coloring probability and (b) forward transition rates as a function of x along the rod. Dots and triangles represent the values obtained from the sampling procedure, while lines represent the expected theoretical values. The binary homogeneous Markov mixture is characterized by rates $\rho_{0,1} = 10/99$, $\rho_{1,0} = 10/11$, with initial condition $p_0(-L/2) = 0.9$. Error bars are computed according to Eq. (11).

estimator the marker function $\mathbb{1}_\alpha(x)$, i.e., the function that is equal to one if the material at position x is α , and zero otherwise. Thus, the ensemble-averaged $\mathbb{1}_\alpha(x)$, namely,

$$\overline{\mathbb{1}_\alpha}(x) = \frac{1}{M} \sum_{m=1}^M (\mathbb{1}_\alpha)_m(x) \quad (12)$$

yields a fair estimate of the coloring probability, which converges to $p_\alpha(x)$ for $M \rightarrow \infty$. For the latter, an estimator is built by dividing the rod into small segments of length dx_k , centered at x_k , and counting the number $n_{\alpha \rightarrow \beta}(x_k, \Omega_\pm)$ of oriented color transitions $\alpha \rightarrow \beta$ falling within each segment. The quantity

$$\overline{n_{\alpha \rightarrow \beta}}(x_k, \Omega_\pm) = \frac{1}{M} \sum_{m=1}^M (n_{\alpha \rightarrow \beta})_m(x_k, \Omega_\pm) \quad (13)$$

yields a fair estimate of the transition rates weighted by the coloring probability, which converges to $\rho_{\alpha,\beta}(x_k, \Omega_\pm)p_\alpha(x_k)$ for $M \rightarrow \infty$ and $dx_k \rightarrow 0$. If the Markov media have been sampled by forward sweeping, the ratio of $\overline{n_{\alpha \rightarrow \beta}}(x_k, \Omega_+)/\overline{\mathbb{1}_\alpha}(x_k)$ is directly compared with the imposed $\rho_{\alpha,\beta}(x, \Omega_+)$, while sampled backward quantities are compared with the ones obtained by means of the symmetry property in Eq. (5).

Figure 2 shows the results obtained using $M = 10^5$ realizations for spatially homogeneous binary mixing statistics for a rod of length $L = 20$ with transition rates $\rho_{0,1} = 10/99$ and $\rho_{1,0} = 10/11$, and initial condition $p_0(-L/2) = 0.9$ corresponding to an equilibrium condition at the left boundary. This mixing statistics is taken from Table II of Ref. [39]. A very good agreement is found between the ensemble-averaged and the theoretical values, both for coloring probabilities and transition rates. Since the mixture is homogeneous and the initial condition is set to the equilibrium condition, these quantities are constant along the rod and do not depend on x . Backward rates are not reported, for the sake of conciseness, but their behavior is similar to direct rates.

In order to probe spatially heterogeneous mixtures, let us now consider ramplike transition rates of the form

$$\rho_{\alpha,\beta}(x, \Omega_+) = \begin{cases} \gamma_{\alpha,\beta}, & x \in \left[-\frac{L}{2}, -\frac{L}{2} + \frac{L}{d_{\alpha,\beta}}\right) \\ \gamma_{\alpha,\beta} + m_{\alpha,\beta} \frac{\left(\frac{L}{2} - \frac{L}{d_{\alpha,\beta}} + x\right)}{\left(L - 2\frac{L}{d_{\alpha,\beta}}\right)}, & x \in \left[-\frac{L}{2} + \frac{L}{d_{\alpha,\beta}}, \frac{L}{2} - \frac{L}{d_{\alpha,\beta}}\right) \\ \gamma_{\alpha,\beta} + m_{\alpha,\beta}, & x \in \left[\frac{L}{2} - \frac{L}{d_{\alpha,\beta}}, \frac{L}{2}\right]. \end{cases} \quad (14)$$

We define a mixture over a rod of length $L = 20$, where $\rho_{0,1}(x, \Omega_+)$ obeys Eq. (14) with the coefficients $\gamma_{0,1} = 10/99$, $m_{0,1} = 0.5$, and $d_{0,1} = 5$, respectively. The rate $\rho_{1,0} = 10/11$ is taken constant along the rod, and the initial condition $p_0(-L/2) = 0.9$ is chosen to ensure the equilibrium at the left boundary. As before, 10^5 realizations are sampled, and the estimated color probabilities and reaction rates are compared to theoretical predictions. Results are reported in Figs. 3(a), 3(b), and 3(c). Overall, a good agreement is found between the theoretical and ensemble-averaged values, confirming the reliability and the robustness of the algorithm used to generate Markov media. In particular, ensemble-averaged forward rates converge to the rates used for sweeping, and ensemble-averaged backward rates converge to the values computed from Eq. (5). Furthermore, Fig. 3(c) shows that forward and backward transition rates for the case $1 \rightarrow 0$ dramatically differ.

A further test is conducted to understand the behavior of the system when the spatial gradient becomes steep. For this purpose, binary Markov media are sampled using the transition rates given by Eq. (14) in the limit $d_{\alpha,\beta} \rightarrow 2$. We consider in particular the ‘‘color flip’’ case, where $\rho_{0,1}$ and $\rho_{1,0}$ swap at $x = 0$. Correspondingly, the transition rates read

$$\rho_{0,1}(x, \Omega_+) = \begin{cases} \frac{10}{99}, & x \in \left[-\frac{L}{2}, 0\right) \\ \frac{10}{11}, & x \in \left[0, \frac{L}{2}\right] \end{cases}, \quad (15)$$

$$\rho_{1,0}(x, \Omega_+) = \begin{cases} \frac{10}{11}, & x \in \left[-\frac{L}{2}, 0\right) \\ \frac{10}{99}, & x \in \left[0, \frac{L}{2}\right] \end{cases}, \quad (16)$$

given with the initial condition $p_0(-L/2) = 0.9$ which ensures the equilibrium condition at $x = -L/2$. This case is illustrated in Fig. 4: a good agreement is found between the theoretical results and the sampled values.

In order to go beyond the special case of binary mixing statistics, we have also explored N -ary Markov media. An example with three different material phases has been

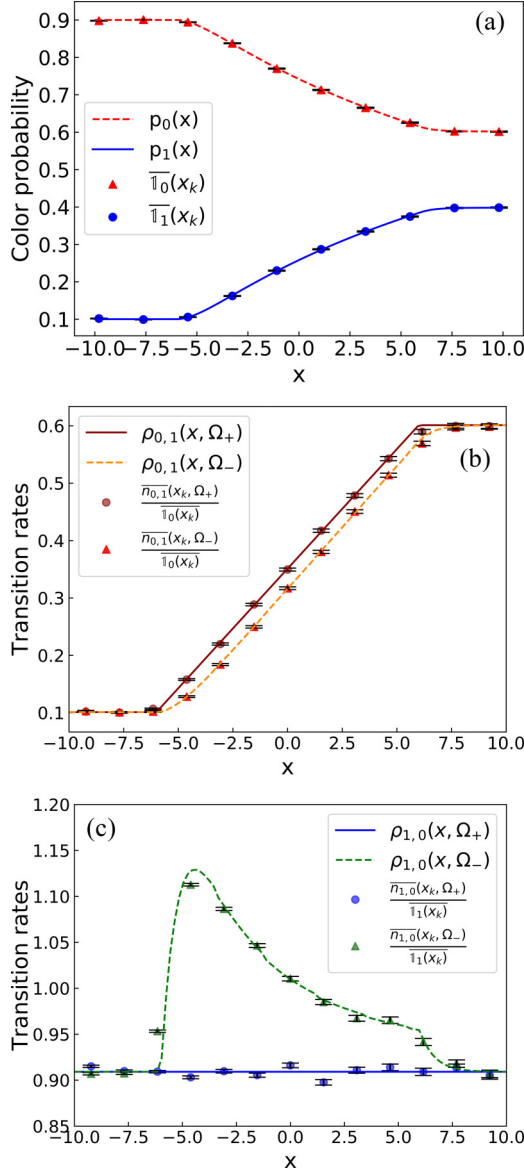


FIG. 3. (a) Coloring probability, (b) transition rates $0 \rightarrow 1$, (c) transition rates $1 \rightarrow 0$ as a function of the position x along the rod. Dots and triangles represent the values obtained from the sampling procedure, and lines represent the expected theoretical values. The forward transition rates $\rho_{0,1}$ (used for sweeping) follow the ramplike function given in Eq. (14), with parameters $y_{0,1} = 10/99$, $m_{0,1} = 0.5$, $d_{0,1} = 5$, and $\rho_{1,0}$ is constant along the rod with value $10/11$. Error bars are computed according to Eq. (11).

tested for a segment of length $L = 20$ with ramplike transition rates as given in Eq. (14). The chosen parameters are reported in Table I, and the corresponding initial conditions

TABLE I. Input parameters of Eq. (14) used to sample ternary Markov media.

α, β	0,1	0,2	1,0	1,2	2,0	2,1
$y_{\alpha,\beta}$	100/99	100/88	100/11	100/77	100/22	100/11
$m_{\alpha,\beta}$	6	5	-6	5	-4	-5
$d_{\alpha,\beta}$	5	5	7	7	4	4

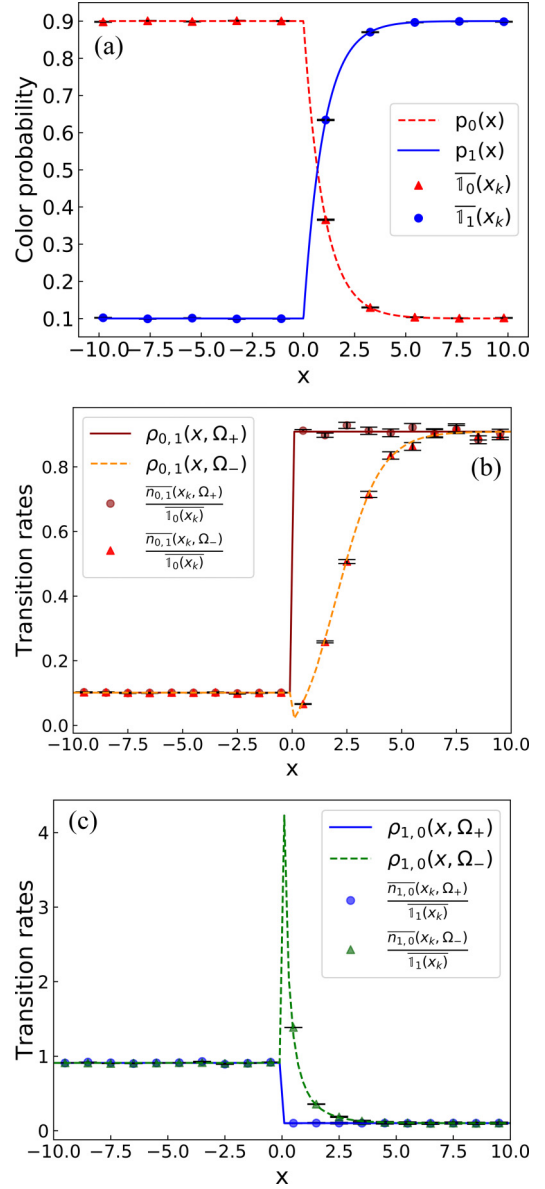


FIG. 4. (a) Coloring probability, (b) transition rates $0 \rightarrow 1$, (c) transition rates $1 \rightarrow 0$ as a function of the position x along the rod. Dots and triangles represent the values obtained from the sampling procedure, and lines represent the expected theoretical values. The input transition rates (used for sweeping) are given by Eqs. (15) and (16). Error bars are computed according to Eq. (11).

have been chosen to preserve equilibrium at the left boundary of the rod: solving the system of Eqs. (8) coupled with the condition $\sum_{\alpha} p_{\alpha} = 1$ yields the values $p_0(-L/2) = 0.777$, $p_1(-L/2) = 0.144$, and $p_2(-L/2) = 0.079$. As before, an ensemble of $M = 10^5$ realizations is sampled. The estimated coloring probability along the rod agrees well with the theoretical prediction from Eq. (4), as illustrated in Fig. 5.

III. ANALYSIS OF PARTICLE TRANSPORT IN MARKOV MEDIA

After assessing the general features of Markov media, we focus now on particle transport problems.

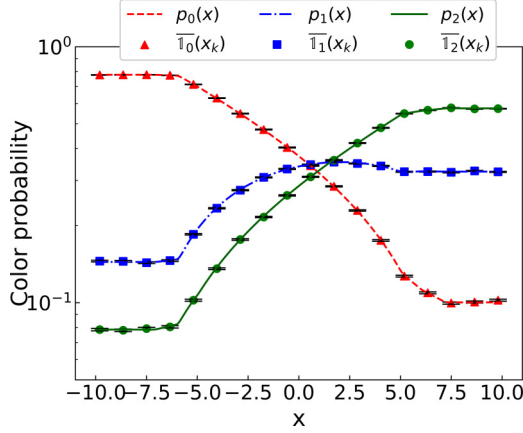


FIG. 5. Coloring probability as a function of the position x along the rod. Dots, triangles, and squares represent the ensemble averages resulting from realizations, and lines represent the expected theoretical values. The ternary heterogeneous Markov mixture is characterized by the mixing statistics given by Eq. (14), whose coefficients are reported in Table I. Error bars are computed according to Eq. (11).

A. Reference solutions

A Monte Carlo code which solves the Boltzmann equation in one-dimensional Markov mixtures has been developed, in order to provide reference solutions to be then compared with CLS. Formally, for each realization m , this code solves the time-independent Boltzmann equation

$$\left\{ \Omega_{\pm} \frac{\partial}{\partial x} + \Sigma_t^{(m)}(x) \right\} \varphi^{(m)}(x, \Omega_{\pm}) = \frac{\Sigma_s^{(m)}(x)}{2} \Phi^{(m)}(x) + Q^{(m)}(x, \Omega_{\pm}), \quad (17)$$

where $\varphi(x, \Omega)$ is the angular particle flux, $\Phi^{(m)}(x) = \varphi^{(m)}(x, \Omega_+) + \varphi^{(m)}(x, \Omega_-)$ is the scalar particle flux, Σ_t and Σ_s are the total and scattering cross sections, respectively, and Q the source term. We assume that particles are constrained to move along the line, which means that their direction can only take values $\Omega_{\pm} = \pm 1$. This corresponds to the well-known “rod model” [40], whereupon Eq. (17) reduces to a set of two coupled first-order ordinary differential equations for $\varphi^{(m)}(x, \Omega_{\pm})$. To simplify matters further, scattering has been taken isotropic.

The code takes as input the cross sections $\Sigma_{r,\alpha}$ for reaction r within each material α and the source distribution Q . Within each material chunk, material properties are constant, and particle tracking is standard. Flight distances are sampled from exponential distributions with parameter $\Sigma_{t,\alpha}$; if the sampled flight is shorter than the distance to the material interface, the particle is displaced and a collision is sampled. In our model, a collision can be either absorption (with probability $1 - \Sigma_{s,\alpha}/\Sigma_{t,\alpha}$) or isotropic scattering. Otherwise, the particle is moved to the interface and a tentative flight length in the new material (keeping the same direction) is sampled. The process is repeated until the particle is absorbed or leaks from the boundaries.

For each realization m , transport-related observables are estimated by simulating N particle histories. The average

value is estimated using

$$\overline{O_m} = \frac{1}{N} \sum_{i=1}^N O_{m,i}, \quad (18)$$

with related statistical uncertainty

$$\sigma_O^2(\overline{O_m}) = \frac{1}{N-1} \left[\frac{1}{N} \sum_{i=1}^N O_{m,i}^2 - \overline{O_m}^2 \right]. \quad (19)$$

Finally, the ensemble average over the M Markov media realizations is computed using Eq. (10), and the associated uncertainty is estimated by summing the component due to the statistical dispersion of stochastic particle contributions in each realization (stemming from using Monte Carlo to solve the Boltzmann equation) and the one due to the dispersion of the realizations [41].

For our work, the observables of interest are the ensemble-averaged scalar (i.e., direction-integrated) particle flux $\langle \varphi_{\alpha}(x) \rangle$ in each material α , and the particle current through the boundaries of the domain. The flux is estimated using track-length and collision-based estimators over a spatial mesh; currents are estimated by counting the number of flights across the boundaries.

Our Monte Carlo code has been benchmarked against the results presented in Refs. [20,39], where the rod model was solved for each realization using deterministic solvers, providing reference solutions for the transmission and reflection coefficients in binary Markov mixtures with a point source at the left boundary. We revisited the configurations proposed in those works for several rod lengths, transition rates, and material cross sections. For all the tested configurations, a very good agreement was found between our simulations and published results, with maximum discrepancy below 1%.

B. A modified CLS method with memory effects

The Levermore-Pomraning equations are a set of coupled Boltzmann-like transport equations describing the ensemble-averaged angular particle flux $\psi_{\alpha}(x, \Omega_{\pm})$ in material α [4]. It has been shown that the ensemble-averaging procedure leads to an infinite hierarchy of increasingly singular equations for the moments of the angular flux: the Levermore-Pomraning (LP) equations are established by truncating the hierarchy at the first order, under the assumption of Markov mixing statistics. For the rod model with isotropic scattering, this procedure yields

$$\left\{ \Omega_{\pm} \frac{\partial}{\partial x} + \Sigma_{t,\alpha}(x) + \rho_{\alpha}(x, \Omega_{\pm}) \right\} \psi_{\alpha}(x, \Omega_{\pm}) = \frac{\Sigma_{s,\alpha}}{2} \Psi_{\alpha}(x) + \sum_{\beta \neq \alpha} \rho_{\beta,\alpha}(x, \Omega_{\pm}) \psi_{\beta}(x, \Omega_{\pm}) + Q_{\alpha}(x, \Omega_{\pm}), \quad (20)$$

where $\Psi_{\alpha}(x) = \psi_{\alpha}(x, \Omega_+) + \psi_{\alpha}(x, \Omega_-)$ is the ensemble-averaged scalar particle flux. The LP equations are approximate, unless the medium is purely absorbing, in which case they are known to be exact [4]. It has been shown that Eqs. (20) can be given a probabilistic meaning [42], which in turns leads to the CLS approach [24]. The LP equations formally describe the average density of particles having an

additional phase-space coordinate α , assigned at the source. Particles undergo flights with a modified total cross section $\Sigma_{t,\alpha}^*(x, \Omega_{\pm}) = \Sigma_{t,\alpha}(x) + \rho_{\alpha}(x, \Omega_{\pm})$ and can switch color label with probability $\rho_{\alpha}(x, \Omega_{\pm})/\Sigma_{t,\alpha}^*(x, \Omega_{\pm})$ at the end of each flight. This interpretation lends itself to a Monte Carlo sampling strategy. Since the color switch is memoryless, due to the Markov nature of the underlying stochastic process, the CLS approach (and equivalently the LP equations) cannot preserve the spatial correlations of the media, which is ultimately responsible for the discrepancy with respect to the reference ensemble-averaged solutions [22,30]. This is particularly relevant for diffusing media, where particles can be back-scattered and “see” a material interface that had already been crossed.

For the special case of spatially homogeneous Markov media, the pioneering work of Adams and Zimmerman introduced a CLS algorithm featuring three different layers of memory effect: instead of immediately forgetting the position of the sampled interface between colors during a flight, the past interface or the two past interfaces are preserved and re-sampled only when the particle first leaves the current material chunk [23,24]. Strategies characterized by one or two levels of memory were called algorithms B and C, respectively. Recently, algorithms B and C have been extended to three-dimensional spatially uniform settings, using the Poisson-Box Sampling [31] and the Local Realization Preserving [32] methods.

The accuracy of standard CLS in spatially heterogeneous media has been probed both in one-dimensional [33,34] and three-dimensional configurations [35]. As a stepping stone towards the development of a general CLS-like algorithm including memory effects and adapted to spatially heterogeneous media in arbitrary dimension, in this work we examine the simpler case of one-dimensional heterogeneous configurations.

For this purpose, a Monte Carlo code has been developed, whose implementation is briefly discussed in the following.

1. Algorithm A

For the sake of comparison, our code can also sample Algorithm A, i.e., the standard version of CLS without memory effects. The sampling strategy closely follows [24], the main difference being that the rates $\rho_{\alpha,\beta}(x, \Omega_{\pm})$ are now space and direction-dependent, and is here recalled since it provides the basis for algorithms with memory:

(1) The initial coordinates of the particle are sampled from Q_{α} : in addition to choosing the starting position and direction, the particle is also assigned a color α .

(2) An interaction distance l is sampled from a non-homogeneous exponential probability density function with modified total cross section:

$$\Sigma_{t,\alpha}^*(x, \Omega_{\pm}) = \Sigma_{t,\alpha} + \rho_{\alpha}(x, \Omega_{\pm}). \quad (21)$$

The total transition rate $\rho_{\alpha}(x, \Omega_{\pm})$ appearing in the modified total cross section accounts for the effects of the random media on the particle displacements, and depends on the particle direction Ω_{\pm} .

(3) The particle is moved to the interaction point and a collision event is sampled. The collision can be either absorp-

tion, isotropic scattering or color change. The probability for one of these events to happen is given by the ratio $\Sigma_{r,\alpha}/\Sigma_{t,\alpha}^*$, where $\Sigma_{r,\alpha}$ is the cross section for the event r . For the color change, this corresponds to $\rho_{\alpha}(x, \Omega_{\pm})$: the particle disappears as α and reappears as $\beta \neq \alpha$ at the same location and with the same direction. The color β is sampled according to

$$P_{\alpha,\beta}(x, \Omega_{\pm}) = \frac{\rho_{\alpha,\beta}(x, \Omega_{\pm})}{\rho_{\alpha}(x, \Omega_{\pm})}. \quad (22)$$

(4) The process is repeated until the particle is either absorbed or leaves the viable domain.

The correct implementation of the algorithm has been verified against the benchmark results reported in Refs. [20,39] (see “model” or “phenomenological results” in the quoted references). Discrepancies lower than 1% with respect to published results confirmed the reliability of our code.

2. Algorithm B

Algorithm B stems from Algorithm A with the addition of one level of memory, and works as follows:

(1) The initial coordinates of the particle are sampled from Q_{α} : in addition to choosing the starting position and direction, the particle is also assigned a color α .

(2) Two spatial coordinates, x_- and x_+ , are sampled from two nonhomogeneous exponential distributions centered on the starting position and having parameters $\rho_{\alpha}(x, \Omega_-)$ and $\rho_{\alpha}(x, \Omega_+)$, respectively. These coordinates represent the two boundaries of the “box” (of material α) surrounding the initial particle position.

(3) An interaction distance l is sampled from an exponential probability density function with total cross section $\Sigma_{t,\alpha}$; at the end of a flight, the particle can either be absorbed or undergo scattering. The probability for one of these events to happen is given by the ratio $\Sigma_{r,\alpha}/\Sigma_{t,\alpha}$, where $\Sigma_{r,\alpha}$ is the cross section for the event r . This procedure is repeated until the particle is absorbed, leaks from the domain, or leaves the box boundaries (x_- or x_+).

(4) If the particle leaves the box boundaries, a new color β is sampled from the space and direction-dependent probability given in Eq. (22), and a new box boundary is sampled using the total transition rate of the new color $\rho_{\beta}(x, \Omega_{\pm})$. For instance, if the particle reaches the right boundary x_+ , x_- is set equal to x_+ and a new x_+ is sampled using $\rho_{\beta}(x, \Omega_+)$. The previous boundary is deleted from the memory.

(5) The transport process is repeated in the new box.

We stress that this version of algorithm B requires minimal modifications with respect to the version proposed by Zimmerman and Adams for spatially homogeneous media: the key point is that all the rates $\rho_{\alpha,\beta}(x, \Omega_{\pm})$ are now space and direction-dependent, which allows entirely preserving the strategy for the sampling of the box interfaces proposed in Refs. [23,24].

3. Algorithm C

Algorithm C includes two levels of memory, and works as follows:

(1) The initial coordinates of the particle are sampled from Q_{α} : in addition to choosing the starting position and direction, the particle is also assigned a color α .

(2) Two spatial coordinates, x_- and x_+ , are sampled from two nonhomogeneous exponential distributions centered on the starting position and having parameters $\rho_\alpha(x, \Omega_-)$ and $\rho_\alpha(x, \Omega_+)$, respectively. These coordinates represent the two boundaries of the “box” (of material α) surrounding the initial particle position.

(3) An interaction distance l is sampled from an exponential probability density function with total cross section $\Sigma_{t,\alpha}$; at the end of a flight, the particle can either be absorbed or undergo scattering. The probability for one of these events to happen is given by the ratio $\Sigma_{r,\alpha}/\Sigma_{t,\alpha}$, where $\Sigma_{r,\alpha}$ is the cross section for the event r . This procedure is repeated until the particle is absorbed, leaks from the domain, or leaves the box boundaries (x_- or x_+).

(4) If the particle leaves the box boundaries, a new color β is sampled from the probability in Eq. (22), and a new set of interfaces x_\pm is sampled using $\rho_\beta(x, \Omega_\pm)$, which yields another box $[x_-, x_c]$ or $[x_c, x_+]$; here x_c denotes the coordinate of the interface of the box through which the particle has left the material chunk α . More precisely, if the particle reaches the boundary $x_-(x_+)$, $x_-(x_+)$ is set equal to x_c and a new position $x_-(x_+)$ is sampled using $\rho_\beta(x, \Omega_{-(+)})$. The opposite boundary $x_+(x_-)$ is retained in memory. As such, the first box is not deleted from the memory, resulting in the preservation of two separate boxes $[x_-, x_c]$ and $[x_c, x_+]$, each distinguished by its own material properties.

(5) Within the two boxes, the particle scatters or is absorbed according to the material properties of each. If the particle crosses the internal box interface x_c , it will switch color and resample a new distance to collision. If the particle crosses the external boundaries x_- or x_+ , another box boundary is sampled, deleting the box on the opposite side.

Similarly as for algorithm B, algorithm C also requires minimal modifications with respect to the version proposed by Zimmerman and Adams for spatially homogeneous media: the strategy for the sampling of the box interfaces is preserved, but the rates become space and direction-dependent.

IV. SIMULATION RESULTS

In order to assess the accuracy of the modified CLS method proposed in the previous sections, we compare it to reference solutions. For this purpose, we choose as fiducial quantities the scalar material fluxes $\langle\varphi_\alpha\rangle$ and the reflection $\langle R\rangle$ and transmission $\langle T\rangle$ coefficients. We consider different configurations, with and without spatial gradients, and with and without absorption.

The first configuration is the spatially heterogeneous Markov binary mixture used in the benchmark presented in Sec. II B, whose ramplike transition rates $\rho_{0,1}(x, \Omega_+)$ are given by Eq. (14), with parameters $y_{0,1} = 10/99$, $m_{0,1} = 0.5$, $d_{0,1} = 5$; the rate $\rho_{1,0}(x, \Omega_+) = 10/11$ is taken constant along the rod. Figure 3 shows the direct and inverse transition rates as a function of x (inverse rates are obtained from Eq. (5)). The equilibrium initial condition is $p_0 = 0.9$, and the rod length is $L = 20$. The total cross sections of the two materials are $\Sigma_{0,t} = 10/99$ and $\Sigma_{1,t} = 100/11$, and two different cases are investigated:

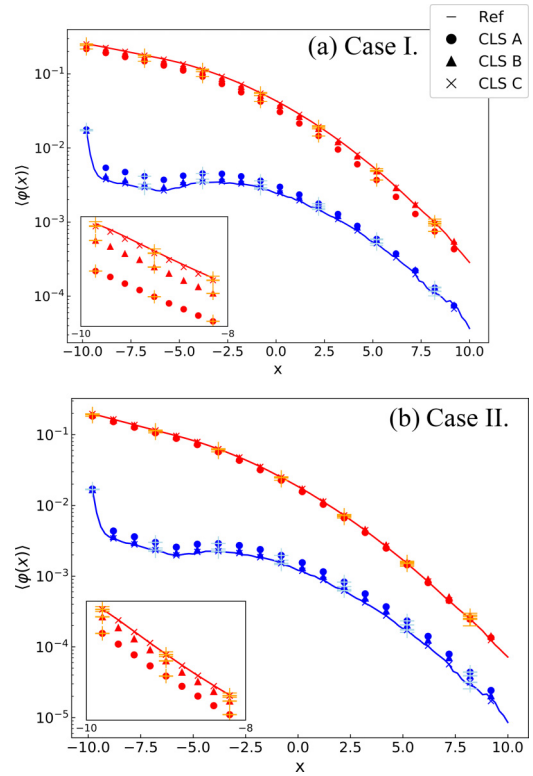


FIG. 6. (a, b) Scalar flux in material 0 (red, upper lines) and 1 (blue, lower lines) as a function of x along the rod, for cases I and II, respectively. Solid line: Reference solutions; dots: algorithm A (memoryless); triangles: algorithm B (one layer of memory effect); crosses: algorithm C (two layers of memory effect).

(1) *Case I*: material 0 is purely scattering, i.e., $\Sigma_{0,s} = \Sigma_{0,t} = 10/99$, while material 1 has $\Sigma_{1,a} = 30/11$ and $\Sigma_{1,s} = 70/11$.

(2) *Case II*: material 0 is purely absorbing, i.e., $\Sigma_{0,a} = \Sigma_{0,t} = 10/99$ and material 1 is the same as in case I.

For both cases, particles start at the left boundary of the rod ($x = -10$) with initial direction $\Omega = +1$. For $x < -5$ the total transition rate of material 0 is of the same order of magnitude as the total cross section, while for $x > -5$ the total transition rate increases and the atomic-mix limit is approached. Conversely, in material 1 the total transition rate is much smaller than the total cross section. For the reference solutions, we sampled $M = 10^5$ material realizations, and $N = 10^6$ histories per realization were simulated. The three CLS algorithms were run with $N = 10^8$ particles.

Simulation results for $\langle R\rangle$ and $\langle T\rangle$ are reported in Table II, while the scalar fluxes in the two materials are shown in Fig. 6. In order to quantify the discrepancy between the CLS algorithms and the reference solutions for the scalar fluxes, we use the chi-square

$$\chi_\alpha^2 = \sum_k \frac{[\langle\varphi_\alpha\rangle(x_k) - \psi_\alpha(x_k)]^2}{\langle\varphi_\alpha\rangle(x_k)}, \quad (23)$$

taken over the spatial bins where the quantities have been tallied. The resulting values are reported in Table II.

Overall, memory effects considerably increase the accuracy of CLS. In fact, for both configurations the discrepancy

TABLE II. Results obtained for cases I and II. The first two columns report the ensemble averages of $\langle R \rangle$ and $\langle T \rangle$, obtained by the simulations on geometric realizations (reference values) and by the CLS algorithms (A, B, and C). The error between CLS and reference is also reported. The third and fourth columns report the values of the chi-square function [Eq. (23)] used to evaluate the discrepancy between the reference and the CLS scalar fluxes in materials 0 and 1, respectively.

	$\langle R \rangle$	$\langle T \rangle$	χ_0^2	χ_1^2
Case I				
Ref.	0.4059 ± 0.0005	0.00147 ± 0.00007		
A	$0.22634 \pm 4 \times 10^{-5}$ Err[%] = 44.24 ± 0.14	$0.001383 \pm 4 \times 10^{-6}$ Err[%] = 5.92 ± 4.85	0.2637	0.0234
B	$0.34074 \pm 5 \times 10^{-5}$ Err[%] = 16.06 ± 0.13	$0.001679 \pm 4 \times 10^{-6}$ Err[%] = 14.21 ± 4.89	0.0308	0.0030
C	$0.39519 \pm 5 \times 10^{-5}$ Err[%] = 2.65 ± 0.13	$0.001436 \pm 4 \times 10^{-6}$ Err[%] = 2.31 ± 4.84	0.0009	0.0001
Case II				
Ref.	0.1232 ± 0.0004	0.00036 ± 0.00002		
A	$0.05420 \pm 2 \times 10^{-5}$ Err[%] = 56.01 ± 0.39	$0.000435 \pm 2 \times 10^{-6}$ Err[%] = 18.14 ± 6.82	0.0291	0.0117
B	$0.10013 \pm 3 \times 10^{-5}$ Err[%] = 18.74 ± 0.34	$0.000441 \pm 2 \times 10^{-6}$ Err[%] = 19.81 ± 6.84	0.0026	0.0013
C	$0.12028 \pm 3 \times 10^{-5}$ Err[%] = 2.39 ± 0.34	$0.000369 \pm 2 \times 10^{-6}$ Err[%] = 0.17 ± 6.71	0.0001	0.0001

between reference solutions and CLS for $\langle R \rangle$ decreases from $\sim 50\%$ (algorithm A) down to $\sim 2\%$ (algorithm C), as shown in Table II. The behavior of scalar fluxes is also better reproduced: the chi-square values decrease by two orders of magnitude between the algorithms A and C, as shown in Table II. Improvements are also seen in the coefficient $\langle T \rangle$, although this quantity is much smaller than $\langle R \rangle$ because of absorption, and thus the error is larger (see Table II).

To complete our analysis, we consider the limit case of purely scattering mixing statistics, where the discrepancy between standard CLS and reference solutions is expected to be amplified. We assume cross sections $\Sigma_{0,t} = \Sigma_{0,s} = 10/99$ and $\Sigma_{1,t} = \Sigma_{1,s} = 100/11$. We examine four different configurations:

Case III: spatially homogeneous Markov mixing with transition rates $\rho_{0,1} = 10/99$ and $\rho_{1,0} = 10/11$, and equilibrium initial condition $p_0 = 0.9$. The rod length is $L = 20$. This configuration has been used in Sec. II B (see Fig. 2), and it is taken from Table II of Ref. [39].

Case IV: spatially heterogeneous Markov mixing with rates equivalent to the ones used in cases I and II.

Case V: spatially heterogeneous Markov mixing with $\rho_{0,1}(x, \Omega_+)$ and $\rho_{1,0}(x, \Omega_+)$ given by Eq. (14), with parameters $y_{0,1} = 10/99$, $m_{0,1} = 0.5$, $d_{0,1} = 5$, and $y_{1,0} = 10/11$, $m_{1,0} = 10$, $d_{1,0} = 5$ ($p_0 = 0.9$ to assign equilibrium at $x = -L/2$).

Case VI: spatially homogeneous Markov mixing characterized by constant transition rates whose values are set to the maximum of the rates of case V, i.e., $\rho_{0,1} = 0.60$ and $\rho_{1,0} = 10.90$, with initial condition $p_0 = 0.947$ to ensure equilibrium at $x = -L/2$.

The simulation results are reported in Table III: memory effects significantly reduce the discrepancy between reference solutions and CLS for $\langle R \rangle$ and $\langle T \rangle$ in cases III, IV, and V. In case III, the total transition rate of material 0 is comparable

to the total cross section, while the ones of material 1 are smaller. Thus, particles have a high probability of being back-scattered and the impact of memory effects is expected to be larger. In cases IV and V, the material chunk size decreases as x increases, approaching the atomic-mix limit for $x > 5$. In particular, in case IV a spatial gradient is imposed in the transition rates of material 0, reducing the chunk size along x [see Fig. 3(b)]. This reduces the probability for scattering to happen in material 0, but it increases the probability of finding material 1, which is a strong scatterer. Therefore, similarly as for case III, memory effects are highly beneficial, especially for the transmission coefficient, whose error decreases from 195.61% (algorithm A) down to 38.92% (algorithm C). Analogous considerations apply to case V, where a strong gradient is imposed to material 1. For large x the chunk size of material 1 decreases (making scattering less probable); for smaller x , scattering remains important and memory effects play an essential role in improving the accuracy of CLS. A significant improvement can be also noticed in the behavior of the scalar fluxes in material 0, as shown in Fig. 7 and by the values of the chi-square in Table III. On the contrary, memory effects seem to be ineffective in increasing the accuracy of the scalar flux in material 1. However, it is important to notice that, in these configurations, the scalar flux in material 1 is of the order of $\sim 10^{-2}$ (in arbitrary units), a value comparable to the deviation between the fluxes predicted by Algorithm A and C for material 0. Memory effects do not enhance the model accuracy at this scale. Finally, in case VI memory effects have also a positive contribution, although their impact is smaller than in the previous cases. This is consistent with the fact that here cross sections are smaller than total transition rates, for both material 0 and 1 along the entire rod. Therefore, in this configuration the atomic mix limit is approached, and CLS becomes closer to the reference solutions. Our findings are

TABLE III. Results obtained for cases III, IV, V, and VI. The first two columns report the ensemble averages of $\langle R \rangle$ and $\langle T \rangle$, obtained by the simulations on geometric realizations (reference values) and by the CLS algorithms (A, B, and C). The error between CLS and reference is also reported. The third and fourth columns report the values of the chi-square function [Eq. (23)] used to evaluate the discrepancy between the reference and the CLS scalar fluxes in materials 0 and 1, respectively.

	$\langle R \rangle$	$\langle T \rangle$	χ_0^2	χ_1^2
Case III				
Ref.	0.8253 ± 0.0005	0.1746 ± 0.0005		
A	$0.68353 \pm 4 \times 10^{-5}$ Err[%] = 17.18 ± 0.07	$0.31646 \pm 4 \times 10^{-5}$ Err[%] = 81.21 ± 0.44	0.3606	0.0192
B	$0.75417 \pm 4 \times 10^{-5}$ Err[%] = 8.62 ± 0.07	$0.24582 \pm 4 \times 10^{-5}$ Err[%] = 40.76 ± 0.37	0.0990	0.0295
C	$0.80953 \pm 4 \times 10^{-5}$ Err[%] = 1.92 ± 0.07	$0.19046 \pm 4 \times 10^{-5}$ Err[%] = 9.06 ± 0.34	0.0043	0.0110
Case IV				
Ref.	0.9480 ± 0.0002	0.05195 ± 0.0002		
A	$0.84641 \pm 4 \times 10^{-5}$ Err[%] = 10.72 ± 0.03	$0.15358 \pm 3 \times 10^{-5}$ Err[%] = 195.61 ± 1.05	0.4211	0.0194
B	$0.88783 \pm 3 \times 10^{-5}$ Err[%] = 6.35 ± 0.03	$0.11216 \pm 3 \times 10^{-5}$ Err[%] = 115.88 ± 0.73	0.1865	0.0191
C	$0.92782 \pm 2 \times 10^{-5}$ Err[%] = 2.13 ± 0.03	$0.07217 \pm 3 \times 10^{-5}$ Err[%] = 38.92 ± 0.51	0.0323	0.0234
Case V				
Ref.	0.8391 ± 0.0004	0.1608 ± 0.0004		
A	$0.75390 \pm 4 \times 10^{-5}$ Err[%] = 10.16 ± 0.05	$0.24609 \pm 4 \times 10^{-5}$ Err[%] = 53.03 ± 0.31	0.3520	0.0481
B	$0.78264 \pm 4 \times 10^{-5}$ Err[%] = 6.74 ± 0.05	$0.21735 \pm 4 \times 10^{-5}$ Err[%] = 35.15 ± 0.29	0.1401	0.0360
C	$0.80662 \pm 4 \times 10^{-5}$ Err[%] = 3.88 ± 0.05	$0.19337 \pm 4 \times 10^{-5}$ Err[%] = 20.24 ± 0.28	0.0345	0.0214
Case VI				
Ref.	0.8385 ± 0.0004	0.1614 ± 0.0004		
A	$0.78816 \pm 4 \times 10^{-5}$ Err[%] = 6.01 ± 0.05	$0.21183 \pm 4 \times 10^{-5}$ Err[%] = 31.24 ± 0.26	0.0384	0.0008
B	$0.80103 \pm 4 \times 10^{-5}$ Err[%] = 4.48 ± 0.05	$0.19896 \pm 4 \times 10^{-5}$ Err[%] = 23.26 ± 0.25	0.0220	0.0013
C	$0.81231 \pm 4 \times 10^{-5}$ Err[%] = 3.13 ± 0.05	$0.18768 \pm 4 \times 10^{-5}$ Err[%] = 16.28 ± 0.25	0.0098	0.0017

consistent with those reported by Zimmerman for spatially homogeneous configurations [Figs. 1(a) and 1(b) of Ref. [23]]: the relative error between CLS and reference solutions in $\langle R \rangle$ and $\langle T \rangle$ decreases from tens of percents (algorithm A) down to a few percents (algorithm C).

The accuracy of CLS algorithms with respect to the ensemble averages $\langle R \rangle$ and $\langle T \rangle$ over Markov media should be put in perspective by considering the full distribution of the observables. For this purpose, in Fig. 8 we display the normalized distributions of the coefficients R and T stemming from Monte Carlo simulations for the benchmark cases I, III, and VI. As a general consideration, highly nonsymmetrical shapes can be observed, especially in cases I and III where bimodality and cutoff effects appear. The behavior of the full distributions aligns with previous findings [29] and is not straightforwardly related to the physical properties and the mixing statistics of the explored configurations. This allows concluding that the average values predicted

by CLS-like algorithms, although relatively close to the ensemble-averaged values, may fail to be representative, similarly as observed in spatially homogeneous low-dimensional configurations [1,29]. A possible way of overcoming this issue would be to establish CLS-like equations for the higher moments of the observables, and in particular the variance: it should be noted, however, that such attempts have met only limited success for the simpler case of spatially homogeneous media [43].

V. CONCLUSIONS

In this paper we have proposed a class of modified CLS-like algorithms for particle transport in Markov media. These methods are capable of taking into account memory effects in general spatially heterogeneous settings. The effectiveness and the robustness of the developed models have been evaluated against reference solutions obtained by taking ensemble

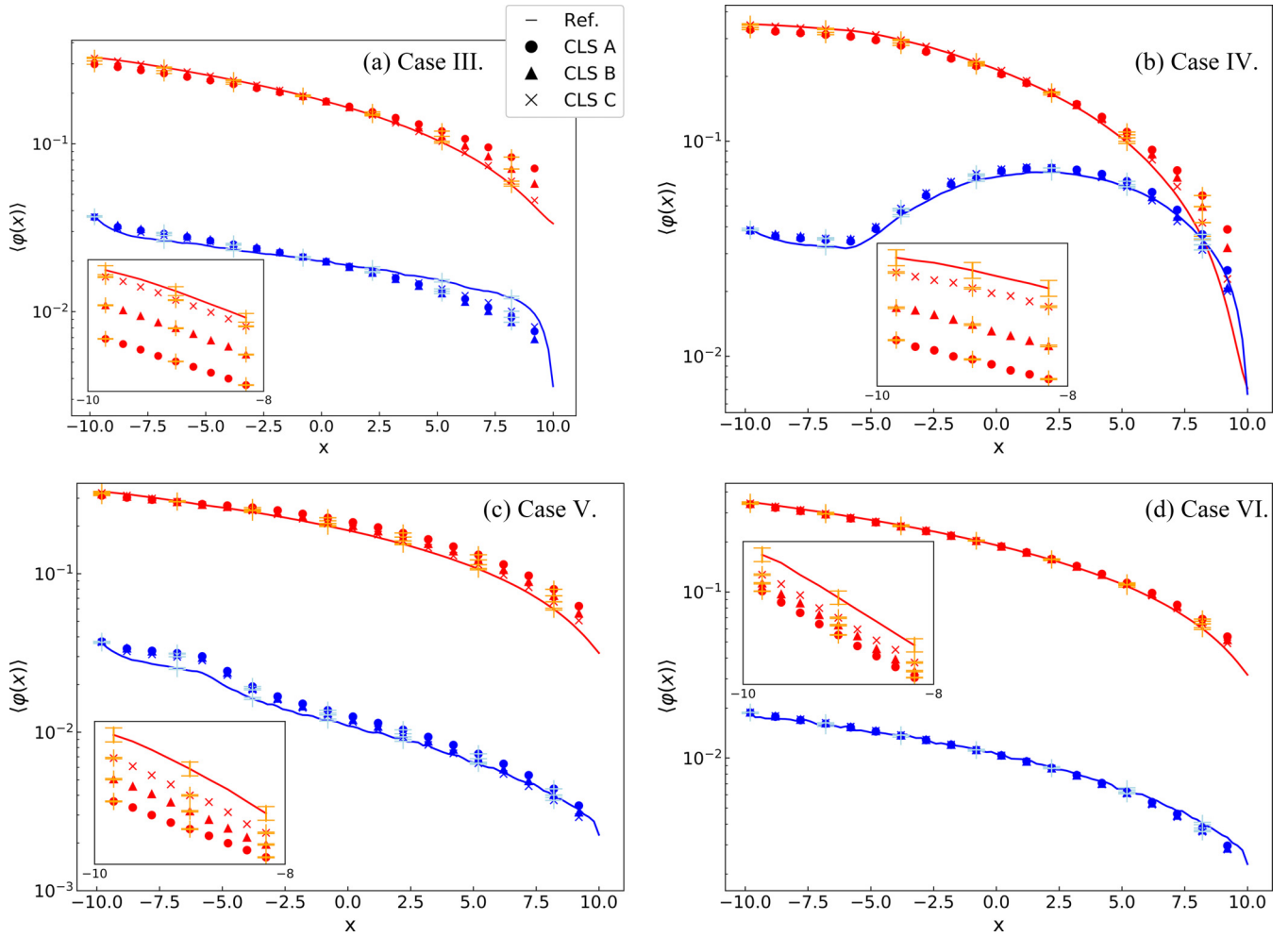


FIG. 7. (a)–(d) Scalar flux in material 0 (red, upper lines) and 1 (blue, lower lines) as a function of x along the rod, for the four simulation cases III, IV, V, and VI, respectively. Solid line: Reference solutions; dots: algorithm A (memoryless); triangles: algorithm B (one layer of memory effect); crosses: algorithm C (two layers of memory effect).

averages over a large collection of Markov media realizations for one-dimensional rod model problems.

We have briefly reviewed the key statistical features of Markov media, which have been then used to probe the reliability of the sampled realizations used for reference solutions. Then we have illustrated how the B and C algorithms of CLS, originally conceived for spatially homogeneous media, can be quite naturally extended to the case of spatially heterogeneous media. In particular, we have shown that the key idea of algorithms B and C, i.e., the use of fictitious “boxes” (one for algorithm B, and two for algorithm C) to preserve partial memory of the past traversed material interfaces, can be straightforwardly adapted to the case of spatially heterogeneous media: the only required modification consists in replacing the constant transition rates with position and direction-dependent rates.

The behavior of the modified CLS was tested against reference solutions for a few relevant benchmark configurations encompassing spatially heterogeneous and spatially homogeneous cases, with and without absorption. The fiducial quantities of the benchmarks were the reflection and transmission coefficients and the material scalar fluxes. Overall, the proposed algorithms perform well, and the presence of mem-

ory effects is beneficial to increase the accuracy of CLS with respect to reference solutions, even in the limit case of configurations without absorption. In this respect, the rod model is particularly challenging, in that the particles have an increased probability of re-crossing the same material interface when they are back-scattered. The effectiveness of modified CLS was evaluated with regard to binary Markov mixtures. Nevertheless, in a forthcoming study will examine how well this algorithm performs in scenarios involving multiple materials.

The Conditional Point Sampling (CoPS) model has been recently proposed as an effective alternative to CLS for one-dimensional Markov media [44–46]. It would be interesting to explore the behavior of CoPS for spatially heterogeneous configurations and compare its performances to those of the modified CLS-strategy discussed here.

Furthermore, future work will focus on extending the strategy presented in this paper to three-dimensional configurations: the idea is to make the Poisson-Box Sampling and the Local Realization Preserving algorithms work in the presence of position and direction-dependent rates. Contrary to one-dimensional configurations, where the particle displacements are trivially aligned with the material interfaces (chords and volumes coincide), in three dimensions the sampling of a

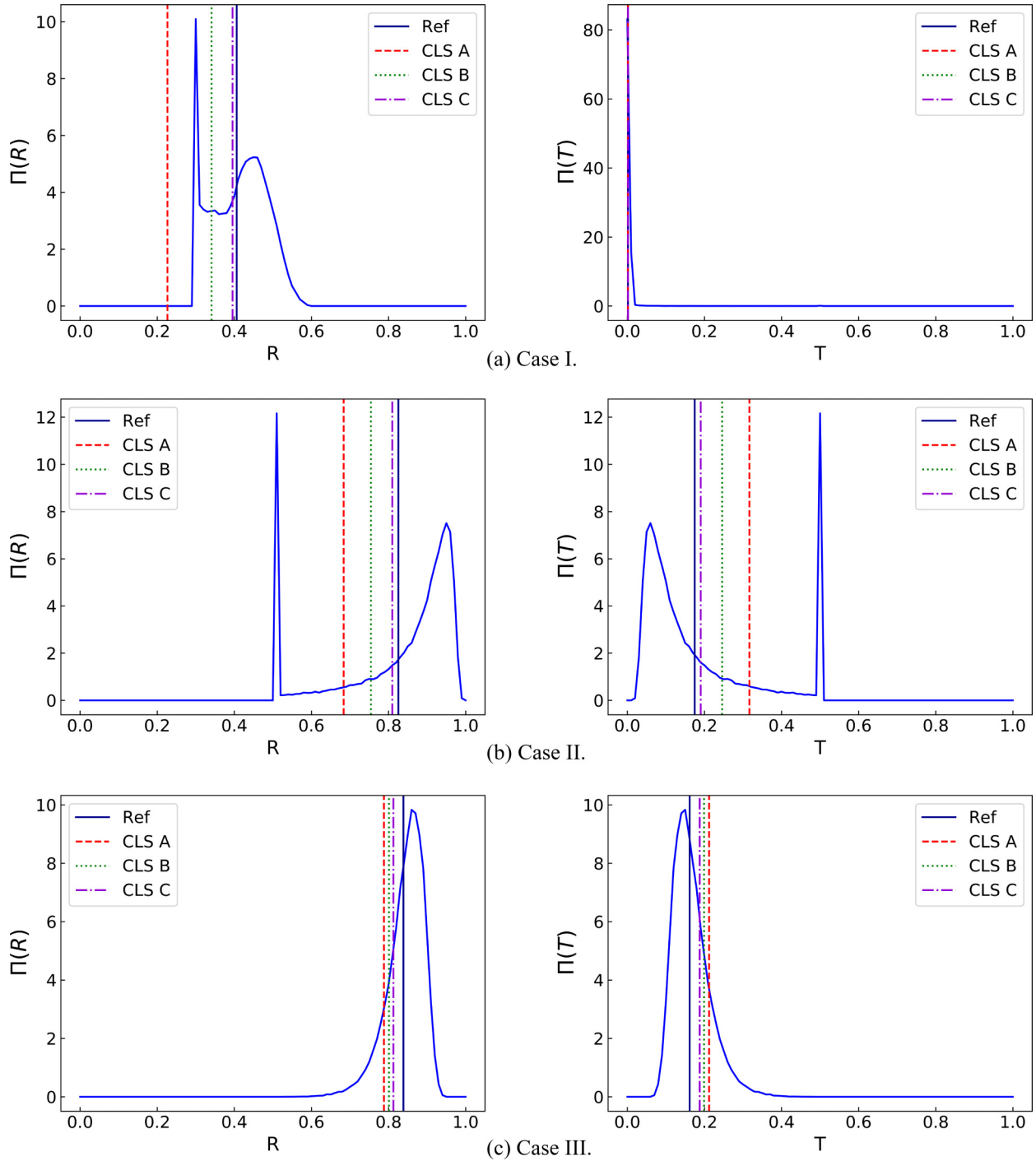


FIG. 8. Analysis of the normalized distribution $\Pi(R)$ of the reflection coefficient R and of the normalized distribution $\Pi(T)$ of the transmission coefficients T , for the benchmark cases I (top), III (center), and VI (bottom). Distributions have been obtained from the reference simulations over the ensemble of sampled stochastic media. Left column: $\Pi(R)$; right column: $\Pi(T)$. The vertical lines denote the average values: blue solid line reference value, red dashed line CLS A, green dotted line CLS B, violet dash-dotted line CLS C.

fititious box to include memory effects requires some care. The possibility of addressing real-world configurations is of utmost importance in view of the industrialization of these methods in the production Monte Carlo code TRIPOLI-4 [47], developed at CEA, which would pave the way, e.g., to applications in the context of ICF [48–50].

The data that support the findings of this study are available from the corresponding author upon reasonable request.

ACKNOWLEDGMENTS

We acknowledge the financial support of the Cross-Disciplinary Program on Numerical Simulation of CEA, the French Alternative Energies and Atomic Energy Commission. The authors express their gratitude to D. Mancusi (CEA) for helpful discussions.

The authors have no conflicts of interest to disclose.

- [1] G. Pomraning, *Linear Kinetic Theory and Particle Transport in Stochastic Mixtures*, Series on Advances in Mathematics for Applied Sciences (World Scientific, Los Angeles, 1991).
- [2] S. Torquato, *Random Heterogeneous Materials: Microstructure and Macroscopic Properties*, Interdisciplinary Applied Mathematics, Vol. 16 (Springer, New York, 2013).
- [3] C. D. Levermore, G. C. Pomraning, D. L. Sanzo, and J. Wong, Linear transport theory in a random medium, *J. Math. Phys.* **27**, 2526 (1986).
- [4] G. Pomraning, Statistics, renewal theory, and particle transport, *J. Quant. Spectrosc. Radiat. Transfer* **42**, 279 (1989).
- [5] D. Vanderhaegen and C. Deutsch, Linear radiation transport in random binary mixtures: A 1D and exact treatment for the scattering case, *J. Stat. Phys.* **54**, 331 (1989).
- [6] G. C. Pomraning, Radiative transfer in Rayleigh–Taylor unstable ICF pellets, *Laser Part. Beams* **8**, 741 (1990).
- [7] D. Vanderhaegen, C. Deutsch, and P. Boissé, Radiative transfer in a one-dimensional fluctuating albedo mixture, *J. Quant. Spectrosc. Radiat. Transfer* **48**, 409 (1992).
- [8] C. D. Levermore and G. B. Zimmerman, Modeling charged particle loss in a fuel/shell mixture, *J. Math. Phys.* **34**, 4725 (1993).
- [9] S. Saito, T. Tanaka, and Y. Sudo, *Design of High Temperature Engineering Test Reactor (HTTR)*, Tech. Rep. JAERI-1332 (Japan Atomic Energy Research Institute, Japan, 1994).
- [10] I. Murata, T. Mori, and M. Nakagawa, Continuous energy Monte Carlo calculations of randomly distributed spherical fuels in high-temperature gas-cooled reactors based on a statistical geometry model, *Nucl. Sci. Eng.* **123**, 96 (1996).
- [11] I. Murata, A. Takahashi, T. Mori, and M. Nakagawa, New sampling method in continuous energy Monte Carlo calculation for pebble bed reactors, *J. Nucl. Sci. Technol.* **34**, 734 (1997).
- [12] F. B. Brown and W. R. Martin, Stochastic geometry capability in MCNP5 for the analysis of particle fuel, *Ann. Nucl. Energy* **31**, 2039 (2004).
- [13] D. J. Behrens, The effect of holes in a reacting material on the passage of neutrons, *Proc. Phys. Soc. A* **62**, 607 (1949).
- [14] P. Aim-O, D. Wongsawaeng, P. Phruksarajanakun, and S. Tancharakorn, Monte Carlo simulation of innovative neutron and photon shielding material composing of high density concrete, waste rubber, lead and boron carbide, *J. Phys.: Conf. Ser.* **860**, 012043 (2017).
- [15] W. R. Burrus, How channeling between chunks raises neutron transmission through boral, *Nucleonics* **16**, 91 (1958).
- [16] W. R. Burrus, *Radiation Transmission through Boral and Similar Heterogeneous Materials Consisting of Randomly Distributed Absorbing Chunks*, Tech. Rep. ORNL-2528 (Oak Ridge National Laboratory, USA, 1960).
- [17] P. Hofmann, Current knowledge on core degradation phenomena, a review, *J. Nucl. Mater.* **270**, 194 (1999).
- [18] C. Larmier, A. Zoia, F. Malvagi, E. Dumonteil, and A. Mazzolo, Neutron multiplication in random media: Reactivity and kinetics parameters, *Ann. Nucl. Energy* **111**, 391 (2018).
- [19] E. Kassianov and D. Veron, Stochastic radiative transfer in Markovian mixtures: Past, present, and future, *J. Quant. Spectrosc. Radiat. Transfer* **112**, 566 (2011).
- [20] M. Adams, E. Larsen, and G. Pomraning, Benchmark results for particle transport in a binary Markov statistical medium, *J. Quant. Spectrosc. Radiat. Transfer* **42**, 253 (1989).
- [21] O. Zuchuat, R. Sanchez, I. Zmijarevic, and F. Malvagi, Transport in renewal statistical media: Benchmarking and comparison with models, *J. Quant. Spectrosc. Radiat. Transfer* **51**, 689 (1994).
- [22] P. S. Brantley, A benchmark comparison of Monte Carlo particle transport algorithms for binary stochastic mixtures, *J. Quant. Spectrosc. Radiat. Transfer* **112**, 599 (2011).
- [23] G. B. Zimmerman, *Recent developments in Monte Carlo techniques*, Tech. Rep. UCRL-JC-105616 (Lawrence Livermore National Laboratory, USA, 1990).
- [24] G. B. Zimmerman and M. L. Adams, Algorithms for Monte Carlo particle transport in binary statistical mixtures, *Trans. Am. Nucl. Soc.* **63**, 287 (1991).
- [25] C. Larmier, E. Dumonteil, F. Malvagi, A. Mazzolo, and A. Zoia, Finite-size effects and percolation properties of Poisson geometries, *Phys. Rev. E* **94**, 012130 (2016).
- [26] C. Larmier, A. Marinosci, and A. Zoia, Chord length distribution in d -dimensional anisotropic Markov media, *J. Quant. Spectrosc. Radiat. Transfer* **224**, 403 (2019).
- [27] C. Larmier, Stochastic particle transport in disordered media: Beyond the Boltzmann equation, Ph.D. thesis, Université Paris-Saclay, France, 2018.
- [28] C. Larmier, A. Zoia, F. Malvagi, E. Dumonteil, and A. Mazzolo, Monte Carlo particle transport in random media: The effects of mixing statistics, *J. Quant. Spectrosc. Radiat. Transfer* **196**, 270 (2017).
- [29] C. Larmier, F.-X. Hugot, F. Malvagi, A. Mazzolo, and A. Zoia, Benchmark solutions for transport in d -dimensional Markov binary mixtures, *J. Quant. Spectrosc. Radiat. Transfer* **189**, 133 (2017).
- [30] C. Larmier, A. Lam, P. Brantley, F. Malvagi, T. Palmer, and A. Zoia, Monte Carlo chord length sampling for d -dimensional Markov binary mixtures, *J. Quant. Spectrosc. Radiat. Transfer* **204**, 256 (2018).
- [31] C. Larmier, A. Zoia, F. Malvagi, E. Dumonteil, and A. Mazzolo, Poisson-Box sampling algorithms for three-dimensional Markov binary mixtures, *J. Quant. Spectrosc. Radiat. Transfer* **206**, 70 (2018).
- [32] P. S. Brantley and G. B. Zimmerman, Benchmark comparisons of Monte Carlo algorithms for three-dimensional binary stochastic media, *Trans. Am. Nucl. Soc.* **117**, 765 (2017).
- [33] A. K. Prinja and P. O' Rourke, *Transport in random media with inhomogeneous mixing statistics*, Tech. Rep. LLNL-SR-750901 (Lawrence Livermore National Laboratory, USA, 2018).
- [34] P. S. Brantley, A. K. Prinja, and P. O' Rourke, *Verification of a Monte Carlo Levermore-Pomraning algorithm for spatially-inhomogeneous binary stochastic media*, Tech. Rep. LLNL-CONF-772027 (Lawrence Livermore National Laboratory, USA, 2019).
- [35] M. A. Kowalski, C. Larmier, F. Madiot, J. Durand, S. Lemaire, and A. Zoia, Particle transport in Markov media with spatial gradients: Comparison between reference solutions and Chord Length Sampling, *J. Quant. Spectrosc. Radiat. Transfer* **286**, 108185 (2022).
- [36] M. A. Kowalski, C. Larmier, and A. Zoia, Analysis of heterogeneous Markov media for particle transport problems, *Phys. Rev. E* **106**, 044108 (2022).
- [37] R. Sanchez, O. Zuchuat, F. Malvagi, and I. Zmijarevic, Symmetry and translations in multimaterial line statistics, *J. Quant. Spectrosc. Radiat. Transfer* **51**, 801 (1994).

- [38] S. Chiu, D. Stoyan, W. Kendall, and J. Mecke, *Stochastic Geometry and Its Applications*, Wiley Series in Probability and Statistics (Wiley, 2013).
- [39] G. Pomraning, Radiative transfer in random media with scattering, *J. Quant. Spectrosc. Radiat. Transfer* **40**, 479 (1988).
- [40] G. Wing, *An Introduction to Transport Theory* (Wiley, 1962).
- [41] T. J. Donovan, T. M. Sutton, and Y. Danon, Implementation of Chord Length Sampling for transport through a binary stochastic mixture, in *Proceedings of Nuclear Mathematical and Computational Sciences: A Century in Review, a Century Anew* (American Nuclear Society, Gatlinburg, TN, 2003).
- [42] D. C. Sahni, Equivalence of generic equation method and the phenomenological model for linear transport problems in a two-state random scattering medium, *J. Math. Phys.* **30**, 1554 (1989).
- [43] G. Pomraning, The variance in stochastic transport problems with Markovian mixing, *J. Quant. Spectrosc. Radiat. Transfer* **56**, 629 (1996).
- [44] E. Vu and A. Olson, *Conditional Point Sampling: A Novel Monte Carlo Method for Radiation Transport in Stochastic Media*, Tech. Rep. SAND2019-2618C (Sandia National Laboratory, USA, 2019).
- [45] E. H. Vu and A. J. Olson, Conditional Point Sampling: A stochastic media transport algorithm with full geometric sampling memory, *J. Quant. Spectrosc. Radiat. Transfer* **272**, 107767 (2021).
- [46] E. H. Vu and A. J. Olson, A limited-memory framework for Conditional Point Sampling for radiation transport in 1D stochastic media, *Nucl. Sci. Eng.* **197**, 212 (2023).
- [47] E. Brun, F. Damian, C. Diop, E. Dumonteil, F. Hugot, C. Jouanne, Y. Lee, F. Malvagi, A. Mazzolo, O. Petit *et al.*, TRIPOLI-4@, CEA, EDF and AREVA reference Monte Carlo code, *Ann. Nucl. Energy* **82**, 151 (2015).
- [48] S. Atzeni, A. Schiavi, and J. R. Davies, Stopping and scattering of relativistic electron beams in dense plasmas and requirements for fast ignition, *Plasma Phys. Controlled Fusion* **51**, 015016 (2009).
- [49] A. Tentori, A. Colaïtis, and D. Batani, 3D Monte-Carlo model to study the transport of hot electrons in the context of inertial confinement fusion. Part I, *Matter Radiat. Extremes* **7**, 065902 (2022).
- [50] A. Tentori, A. Colaïtis, and D. Batani, 3D Monte-Carlo model to study the transport of hot electrons in the context of inertial confinement fusion. Part II, *Matter Radiat. Extremes* **7**, 065903 (2022).